Smart Structures and Systems, Vol. 1, No. 2 (2005) 217-233
DOI: http://dx.doi.org/10.12989/sss.2005.1.2.217

Smart geophysical characterization of particulate materials in a laboratory

Tae-Hyuk Kwon† and Gye-Chun Cho‡

Department of Civil and Environmental Engineering, KAIST, Daejeon 305-701, Korea

(Received July 29, 2004, Accepted April 15, 2005)

Abstract. Elastic and electromagnetic waves can be used to gather important information about particulate materials. To facilitate smart geophysical characterization of particulate materials, their fundamental properties are discussed and experimental procedures are presented for both elastic and electromagnetic waves. The first application is related to the characterization of particulate materials using shear waves, concentrating on changes in effective stress during consolidation, multi-phase phenomena with relation to capillarity, and microscale characteristics of particles. The second application involves electromagnetic waves, focusing on stratigraphy detection in layered soils, estimation of void ratio and its spatial distribution, and conduction in unsaturated soils. Experimental results suggest that shear waves allow studying particle contact phenomena and the evolution of interparticle forces, while electromagnetic waves give insight into the characteristics of the fluid phase and its spatial distribution.

Keywords: electromagnetic wave; particulate material; spatial variability; void ratio; shear wave; small-strain stiffness.

1. Introduction

Small perturbation elastic and electromagnetic waves allow characterization of a soil mass without causing any permanent effect (Santamarina, *et al*. 2001, 2004). The physical interpretation of these measurements (i.e. elastic and electromagnetic wave parameters) permits inferring important information about the soil mass and its processes. Soils are particulate and multi-phase materials (i.e. air, fluid, solid), and soil properties and the interaction among distinct phases can be captured using elastic and electromagnetic wave parameters. This interpretation can be local or global, depending on the scale of interest.

In order to facilitate smart geophysical characterization of particulate materials, their fundamental properties are first discussed, and then experimental procedures are presented for both elastic and electromagnetic waves. The first application is related to the characterization of particulate materials using shear waves while the second application involves electromagnetic waves.

†Graduate Student
‡Assistant Professor, Corresponding Author, Email: gyechun@kaist.ac.kr, Tel: +82-42-869-3622; Fax: +82-42-869-3610

2. Characteristics of particulate materials

The properties of particulate materials are governed by their physical characteristics (e.g. geometry and strength of grain), effective stress, presence of water (e.g. saturated or unsaturated condition), global void ratio (or porosity), temporal scales (e.g. drained or undrained condition), and spatial scales (e.g. fabric, packing) among others. These factors are discussed to gain insight into the fundamental behavior of particulate materials.

2.1. Microscale characteristics

The geometry of a soil grain reflects its chemical composition and formation history and affects soil behavior. Both size and shape are required to properly describe the particle geometry. Particle size is the most relevant parameter in assessing the relative balance between skeletal, electrical and capillary forces between neighboring particles. Particle shape is characterized by three dimensionless ratios: sphericity, roundness and roughness (Wadell 1932, Powers 1953, Krumbein and Sloss 1963, Barrett 1980). Sphericity indicates whether one, two, or three of the particle dimensions are of the same order of magnitude, and it is defined as the diameter of the largest inscribed sphere relative to the diameter of the smallest circumscribed sphere. Roundness is quantified as the average radius of curvature of surface features relative to the radius of the maximum sphere that can be inscribed in the particle. Roughness describes the surface texture relative to the radius of the particle. Convex particle surface profiles can be approximated with a Fourier series or through optical microscopy. Image analyzers can be used to automate particle sizing and shape determination (e.g. Yudhbir and Abedinzadeh 1991, Kuo, *et al*. 1996). The relevance of particle shape on soil strength is intuitively accepted and supported by some experimental evidence. For example, the interparticle friction angle increases with angularity and surface roughness (Frossard 1979, Santamarina and Cascante 1998, Santamarina and Cho 2004).

2.2. Effective stress

When a soil is saturated, the granular skeleton and the pore fluid share the total boundary stress σ applied to a soil mass. The portion carried by the skeleton is the effective stress σ'. If the pore fluid pressure is u, the effective stress σ' is equal to the total stress σ minus the pore fluid pressure u (i.e. $\sigma' = \sigma - u$; Terzaghi's effective stress concept). Following Coulomb's failure criterion (i.e. $\tau = \sigma' \tan \phi$, where ϕ is the friction angle of the soil), the shear strength τ is a function of the effective stress σ' (Heyman 1997). In addition, stiffness (at small or large strain) and dilatancy (i.e. the volume change upon shear may be either positive or negative; Schofield 1998) are related to the effective stress.

2.3. Presence of water

Contrary to saturated soils, the presence of two non-miscible fluids adds interfacial tension (i.e. surface tension) and capillary forces between particles. This is typically the case between air and water, or water and organic fluids. In unsaturated soils, the negative pore-water pressure in menisci that exists due to capillarity at particle contacts increases the interparticle forces, changes the small-strain stiffness, and alters the soil strength (Fredlund and Rahardjo 1993, Cho 2001). All forms of conduction and

diffusion processes depend on the size and connectivity of the menisci as well. Furthermore, the equivalent effective stress due to capillary forces increases with decreasing degree of saturation, decreasing particle size (or increasing specific surface), and increasing coordination of the particles (Cho and Santamarina 2001).

2.4. Void ratio

The void ratio (or porosity) is affected by the grain size distribution of the soil and the particle shape. In general, well-graded soils produce higher maximum densities while platy particles (i.e. clay) have a wider range of densities. According to the critical state soil mechanics approach, the undrained response of a soil is uniquely related to the initial void ratio (Roscoe, *et al*. 1958, Schofield and Wroth 1968). For example, a lower void ratio for a given soil renders a higher undrained shear strength. Thus, the undrained shear strength can be estimated from critical state parameters and the initial void ratio.

2.5. Spatial variation

The spatial variability of soil parameters affects the macroscale soil response. The effects of spatial variability on soil behavior have been studied in the context of geoprocesses such as soil liquefaction (Popescu and Prevost 1996, Popescu, *et al*. 1997), slope instability (Yong, *et al*. 1977, Tonon, *et al*. 2000), seepage (Griffiths and Fenton 1993, Fenton and Griffiths 1996), and settlement (Paice, *et al*. 1996). The inherent variability of soil properties in natural soil deposits can be very large. Spatial variability has an important effect even in relatively small laboratory specimens as well. The presence of multiple internal spatial scales is associated with the development of multiple temporal scales for processes taking place within the medium such as consolidation, permeability, fluctuation of the capillary fringe, chemical diffusion, aging, creep and cementation (Santamarina, *et al*. 2001). For example, the excess pore water pressure that builds up during shear is determined by the rate of pore water pressure generation versus the rate of pore water pressure dissipation. In turn, both mechanisms are related to the spatial variation of void ratio (Dobry and Petrakis 1990). The internal structure of a soil can be characterized using statistical parameters that summarize the average property (e.g. mean) and the variability (e.g. standard deviation). These parameters are used in the common case of particle size distribution but in the less frequently assessed case of void ratio distribution. However, the spatial distribution of the local values can play a critical role in global behavior, even in soil deposits that have the same global statistics (Cho 2001).

3. Elastic wave applications

Small-strain deformations in particulate materials take place at constant fabric (small-strain conditions apply when the strain level is lower than the elastic threshold strain). Under this condition, the soil deformation observed at the macroscale is the integration of contact level deformations. The stiffness of a soil is dependent on the nature of individual particle contacts, the interparticle contact area, and the interparticle forces (e.g. skeletal, electrical, and capillary forces). The Hertz-Mindlin model of contact behavior shows that the stiffness of two spheres in contact is non-linear and stress-dependent. The simplest expression is of the form (Stokoe, *et al*. 1991, Santamarina, *et al*. 2001).

$$V_s = \sqrt{\frac{G}{\rho}} = \alpha\left(\frac{\sigma'_{\text{mean}}}{1\text{kPa}}\right)^{\beta} \quad (1)$$

where V_s is the shear wave velocity [m/s], G is the shear stiffness [kPa] in the small-strain regime, ρ is density [kg/m^3], the α-factor is the shear wave velocity at 1 kPa, σ'_{mean} is the mean state of effective stress in the propagation plane (e.g. $\sigma'_{\text{mean}}=(1+K_o)\ \sigma'_v / 2$ for the $\sigma'_h = K_o\sigma'_v$ condition where σ'_h is the horizontal effective stress, σ'_v is the vertical effective stress and K_o is the lateral earth pressure coefficient), and the β-exponent reflects the sensitivity of V_s to changes in the mean state of effective stress in the propagation plane. The shear wave velocity in particulate materials only depends on the effective interparticle contact forces and the ensuing contact stiffness, but it is not affected by the bulk stiffness of the pore fluid. For this reason, transverse S-waves (i.e. shear waves) are preferred for the characterization of particulate materials as compared to longitudinal *P*-waves (i.e. compression waves). In this section, shear waves are applied to characterize particulate materials, concentrating on changes in effective stress during consolidation, multi-phase phenomena related to capillarity, and microscale characteristics of the particles.

3.1. Effective stress – consolidation

Particle deformation at contacts (exacerbated by angularity), bending of platy particles, and contact slippage (facilitated in smooth particles) determine the deformability of soils under zero-lateral strain K_o-loading. In order to evaluate the changes in effective stress during consolidation, oedometric tests (K_0 condition) were performed on undisturbed Pusan clay specimens (D_{50}=7 μm, G_s=2.71; for its particle size distribution, refer to Fig. 5). Piezoelectric bender elements (i.e. bimorphs; series-type) were mounted on the top and bottom platens to send and to receive shear waves. The bender elements were insulated from unwanted electromagnetic fields by conductive paint coatings, and fixed to the platens in the form of cantilever beams (Fig. 1a). A signal generator (Agilent 33120A) was used to feed a square pulse to the upper bender element. Signals detected with the lower bender element were amplified using a filter-amplifier (Kronheit 3944), and digitized with a digital storage oscilloscope

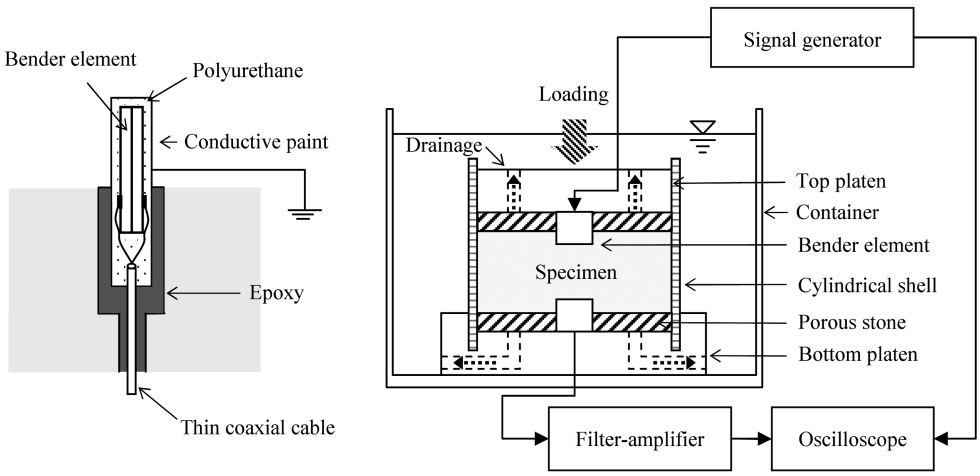

(a) Bender element installation (b) Experimental device

Fig. 1 Schematic drawings of bender elements and experimental set-up

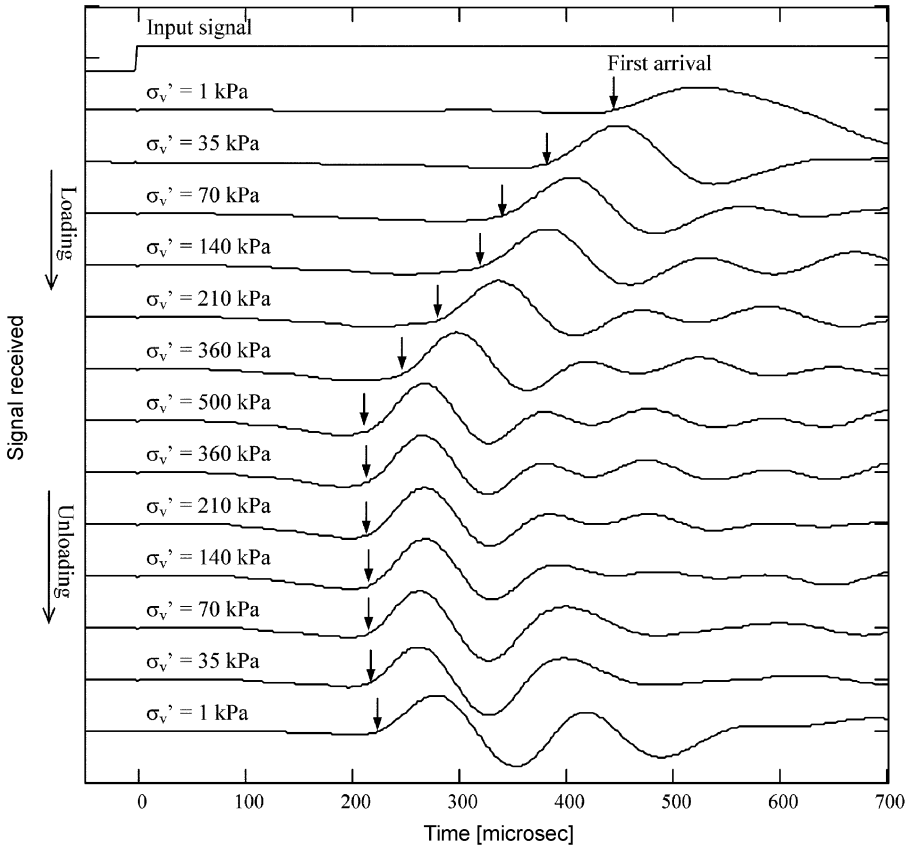

Fig. 2 Typical results of received signals

(Agilent 54622D) as shown in Fig. 1(b). The average of 512 stacked signals was stored on a disk. The volume change of each specimen (diameter = 7.5 cm) was measured at various vertical effective confinements in the range of approximately 1 to 400 kPa.

As a specimen is subjected to a cycle of loading and unloading, the typical results of the received signals are shown in Fig. 2. The first arrival times (marked by arrows) decrease with increasing vertical effective stress during the loading stage. Fig. 3 shows the variation of void ratio and shear wave velocity versus consolidation time under a certain loading where the hollow circles are experimental test results and the solid line is a trend. It seems that the shear wave velocity enables estimating the change in effective stress (i.e. dissipation of excessive pore water pressure) during consolidation. When a soft soil in situ is subjected to additional loading, its consolidation process can be monitored using in-situ shear wave velocities.

Fig. 4 shows the variation of void ratio and shear wave velocity versus applied vertical stress. As the vertical stress increases, the void ratio decreases and the shear wave velocity increases. The empirical relation of shear wave velocity to applied vertical stress is documented in Fig. 4(b), where ϕ is the interparticle friction angle (20^o for the soil used). Experimental results suggest that the shear wave velocity is uniquely related to the state of stress, so that it can be used to assess the state of stress and its change during the consolidation process.

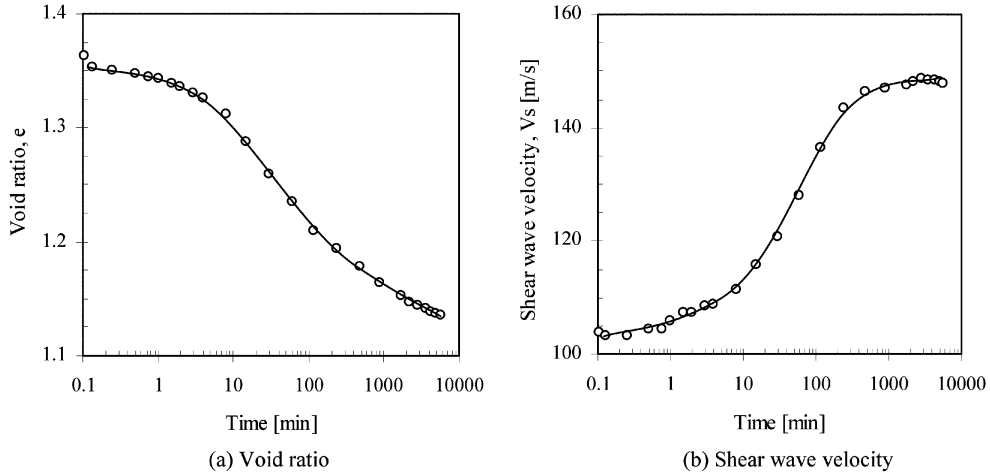

(a) Void ratio (b) Shear wave velocity

Fig. 3 The variation of void ratio and shear wave velocity versus consolidation time

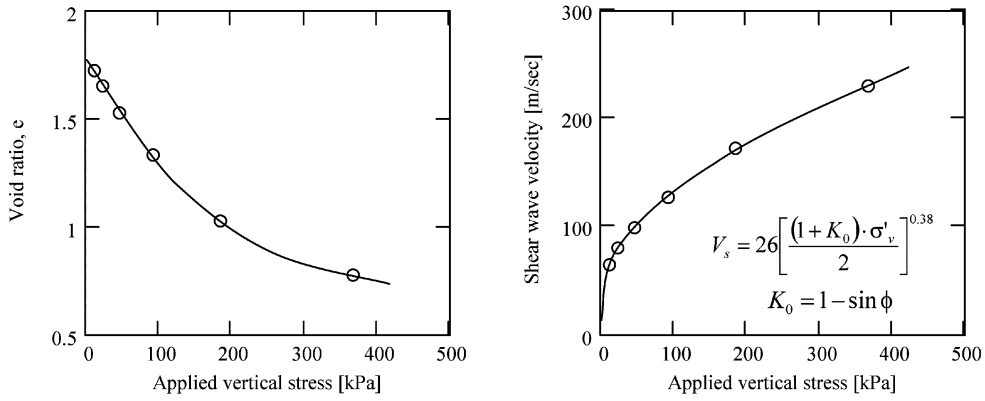

(a) Void ratio (b) Shear wave velocity

Fig. 4 The variation of void ratio and shear wave velocity versus applied vertical stress

3.2. Multi-phase phenomena – capillarity

In order to explore the implications of capillarity on stiffness in unsaturated particulate materials, drying tests were performed while monitoring the saturation of the specimen with shear waves. A drying cell was made for this purpose (Details can be found in Cho and Santamarina 2001). The cell diameter and height were selected as a compromise between accuracy in travel time measurements, side friction, and duration of drying. The Plexiglas shell, the aluminum top platen, and the aluminum bottom platen were all machined with 0.05 mm tolerance. Piezoelectric bender elements were mounted on the top and bottom platens to send and receive shear waves.

The soils tested include a granite powder, a residual soil, Keum River sand, and Pusan clay. Particle size distributions are shown in Fig. 5. The drying cell for the soil specimens was suspended with a flexible wire inside an incubator. The wire acted on an external scale that allowed the weight of the specimen to be monitored, in order to compute the water content or the degree of saturation. The temperature was kept constant at 50°C to avoid changes in surface tension (surface tension decreases with increasing temperature),

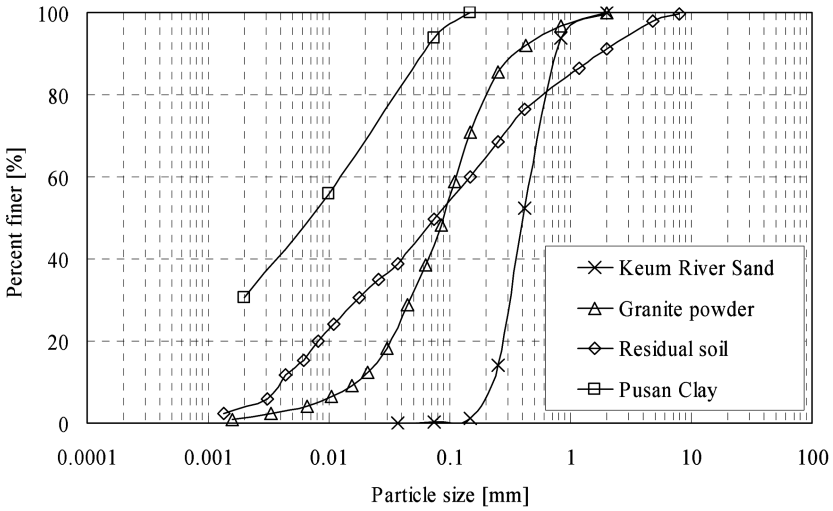

Fig. 5 Particle size distribution

and changes in confinement due to the expansion and shrinkage of the cell.

The measured shear wave velocity is plotted versus the corresponding degree of saturation in Fig. 6. As the degree of saturation decreases from the saturated condition (S = 100%) to the dry condition (S = 0%), the shear wave velocity increases continuously in all of the specimens and shows no drop even at the perfectly dry condition, S = 0% (Fig. 6). The zero degree of saturation is confirmed by measuring the weight of the specimen after further drying at high temperature (i.e. 100^{o}C). The jump in shear wave velocity near S = 0% may be explained by stiffening mechanisms, such as fines migration to the contacts of the larger particles, salt precipitation, and bonding due to ion sharing. The similarity between the grain-size distribution plot (when it is rotated 90^{o}; Fig. 5) and the shear wave velocity plot (Fig. 6) is noticeable, highlighting the importance of the grain-size distribution on capillarity (see also Cho and Santamarina 2001).

In Fig. 6(a), point A is related to the air-entry value in the water-retention curve, which is the air phase breaks through the pore structure. Large pore size governs the magnitude of the effective stress increase in high degrees of saturation. A uniform coarse-grained soil like the Keum river sand tends to have a uniform-sized pore distribution, rendering the gentle slope between points A and C. Point B indicates the transition zone between the funicular (continuous water) and pendular (discontinuous water) stages. Salt precipitation is expected as drying proceeds from the point C to the peak velocity at S = 0%.

In Fig. 6(b), the shear wave velocity for the dry specimen is approximately eight times larger than for the saturated specimen. When the specimen of granite powder is re-saturated by flooding, the shear wave velocity drops to its initial value (square points in Fig. 6b). This result suggests that the light cementation that develops during drying disappears upon wetting.

The variation of shear wave velocity in the residual soil specimen is shown in Fig. 6(c). The shear wave velocity increases continuously and shows no drop at the perfectly dry condition S = 0%. The negative pore-water pressure in the pendular region (at fairly dry condition) causes a strong increase in shear wave velocity.

The variation of shear wave velocity in clay specimens is shown in Fig. 6(d). The shear wave velocity of the undisturbed and remolded specimens increases continuously and shows no drop at the perfectly

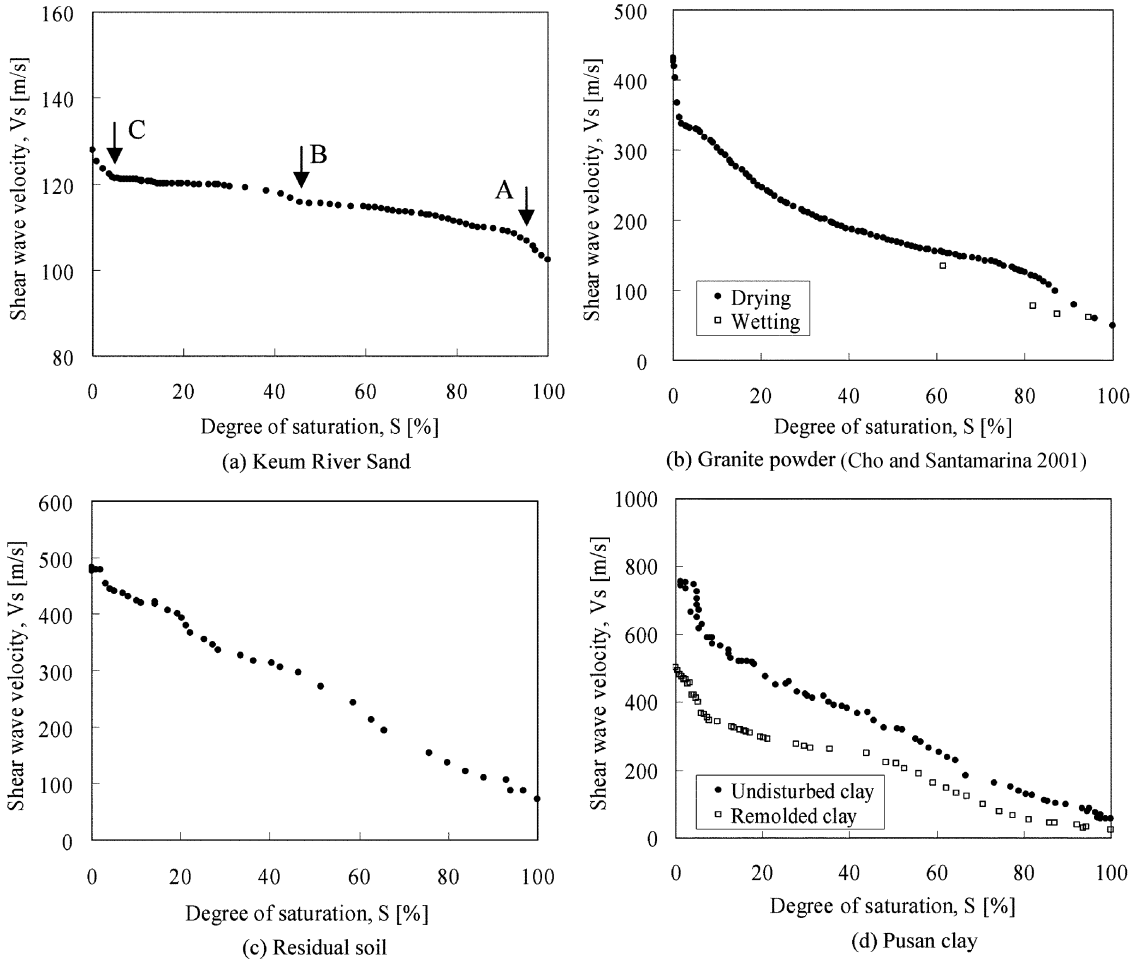

Fig. 6 Shear-wave velocity versus the degree of saturation

dry condition $S = 0\%$. In addition to the stiffening mechanisms, the negative pore-water pressure in the pendular region (at the very low degrees of saturation) causes a strong increase in the shear wave velocity. Meanwhile, the shear wave velocity of the remolded specimen is much lower than that of the undisturbed specimen highlighting the importance of fabric and structure on the evolution of effective stress in unsaturated fine particulate materials.

Overall, experimental results suggest that the shear wave velocity captures the change in effective stress caused by capillarity in unsaturated soils. This is particularly valuable in the pendular regime where direct measurement of the negative pore-water pressure is not feasible.

3.3. Microscale characteristics – particle shape

Spheres with rough surfaces may have the same average contact area as spheres with smooth surfaces, but rough surfaces are composed of many small asperities which can be modeled as cones. The stiffness of a conical contact is smaller than that of a spherical contact because an equivalent

increase in contact area requires more strain in a conical contact. As the force between particles increases, the global spherical shape of the rough particles begins to have a greater influence on the contact behavior than the shape of the asperities, and the stiffness of the rough particle contacts approaches that of a smooth particle. When many different sized asperities are present on particle surfaces, only the largest ones are initially in contact, therefore the actual contact area is lower than in the spherical case and the stiffness is lower (Santamarina and Cascante 1998, Yimsiri and Soga 1999).

Non-spherical, platy or ellipsoidal particles tend to favour the formation of inherently anisotropic fabrics and enhance the development of stress-induced fabric anisotropy. The small-strain longitudinal and shear stiffness reflect fabric anisotropy even under isotropic confinement. The effect of particle orientation on shear wave velocity anisotropy under isotropic effective stress conditions is explored with two sets of specimens; one made of mica flakes and the second prepared with rice grains (Santamarina and Cho 2004). Preferential particle alignment during specimen preparation is readily confirmed in both cases. Experimental results show that the shear wave velocity is higher when the direction of wave propagation is parallel to the main axis of the particles, as compared to the shear wave velocity in specimens where particles are aligned in the direction of particle motion; the ratio $V_{S\text{-}HV}/V_{S\text{-}VH}$ = 1.3-to-1.5 in mica, and $V_{S\text{-}HV}/V_{S\text{-}VH}$ = 1.11 in rice (here the first index represents the direction of wave propagation, the second index represents the direction of particle movement, *H* is the horizontal direction, and *V* is the vertical direction) . Pennington, *et al*. (1997) report similar ranges in shear wave velocity anisotropy in natural clays.

In order to explore the effect of global particle shape on the small-strain behaviour, the shear wave velocity was measured on specimens made of 16 sands with varying confining stresses. The oedometeric cell, shown in Fig. 1, was used for this purpose. Based on experimental results, the α-factor and the β-exponent of Eq. (1) for each sand are determined by best-fitting the data. Fig. 7 shows the effect of particle shape on the shear wave velocity (where Ir is the irregularity defined as the average of sphericity and roundness). In general, a robust inverse trend between the α-factor and the β-exponent is observed in all types of soils: the stiffer the particles and the denser the packing, the higher the value of the factor α and the lower the β-exponent. Experimental results show that as particle shape becomes

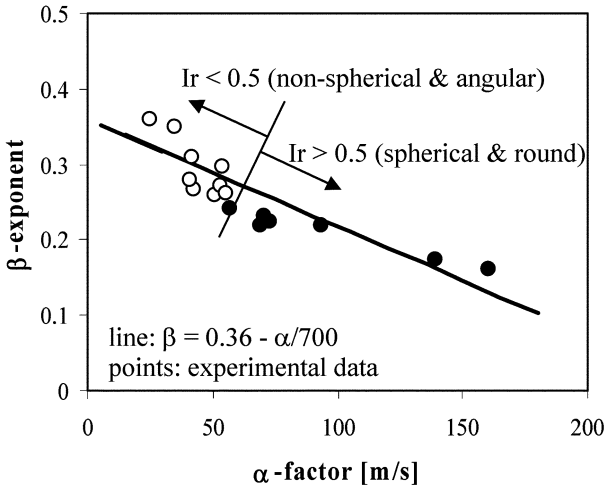

Fig. 7 The effect of particle shape on the shear wave velocity. The α–β trend line is from Santamarina, *et al*. (2001)

non-spherical and angular (Ir<0.5), the exponent β increases with decreasing α factor. Thus, angular and non-spherical particles increase the sensitivity of stiffness to the state of stress.

4. Electromagnetic wave applications

When a particulate medium is subjected to an electromagnetic field, its response is dependent on the electromagnetic properties and the spatial distribution of constituents (i.e. gas, fluid and solid phases), and volume fraction. There are three electromagnetic properties: electrical conductivity σ (or resistivity $\rho = 1/\sigma$), dielectric permittivity ε^*, and magnetic permeability μ^*, where the asterisk means a complex quantity. Electrical conductivity is a measure of charge mobility in response to an electric field. The dielectric permittivity is frequency-dependent, and it consists of a real part ε' and an imaginary part ε'' (i.e. $\varepsilon^* = \varepsilon' + j \cdot \varepsilon''$). The relative dielectric permittivity is the ratio of the dielectric permittivity to the permittivity of vacuum (i.e. $\kappa^* = \varepsilon^*/\varepsilon_0 = \kappa' + j \cdot \kappa''$, where $\varepsilon_0 = 8.85 \cdot 10^{-12}$ F/m and j = the imaginary unit). The real relative dielectric permittivity κ' represents the polarizability of the material, while the imaginary relative permittivity κ'' captures polarization losses. The complex magnetic permeability μ^* captures the magnetizability and the magnetization losses of the material. Most soils are non-ferromagnetic, therefore, the complex permeability μ^* is the permeability of vacuum μ_0 ($\mu^* = \mu_0 = 4\pi \cdot 10^{-7}$ H/m).

The complex permittivity and conductivity reflects the interplay between porosity, volumetric water content, pore fluid characteristics, specific surface, mineralogy and fabric (Santamarina, *et al*. 2001). Conductivity in wet particulate media reflects the contributions of the particle conductivity (generally small), the bulk fluid conductivity, and surface conduction due to the increased counterion concentration in the double layer surrounding the particles. Thus, the connectivity of phases is related to the conductivity of soil-water mixtures, which allows the possible assessment of stratigraphy detection in layered soils and conduction in unsaturated soils. The dielectric permittivity of soil-water mixtures depends on the type of soil, including its specific surface, the characteristics of the fluid, the volumetric fluid content, and the frequency of the applied electric field. Thus, the dielectric permittivity of a soil is closely associated with water content and void ratio. In this section, electromagnetic waves are applied to characterize particulate materials, with emphasis on stratigraphy detection in layered soils, the estimation of void ratio and its spatial distribution, and conduction in unsaturated soils.

4.1. Stratigraphy – layer detection

A simple and effective technique is proposed to assess the spatial variability (including layers) of sandy or clayey soil specimens with sub-millimetric resolution. The technique involves a needle-size probe that is pushed into the soil and permits measuring the local electromagnetic properties of the medium along its path. The device and its calibration are described in detail in Cho, *et al*. (2004). The probe is a thin, stainless steel needle, with an insulated wire inserted into the needle, and bonded to it with epoxy resin to form a coaxial probe. The tip of the probe is ground and polished to form a sharp edge (25 degrees – single side). The dimensions of the probe are: probe diameter is d_{probe} = 2.10 mm, the wire diameter is d_{core} = 0.63 mm, and the probe length is 152 mm. The electromagnetic properties were determined by measuring either the resistance R and the reactance X, or the magnitude of the impedance $|Z|$ and the phase angle θ ($Z^* = R + j \cdot X$) using an HP-4192A Hewlett Packard low frequency impedance analyzer.

The ability of the electrical needle probe to resolve interfaces was explored using sandy and clay

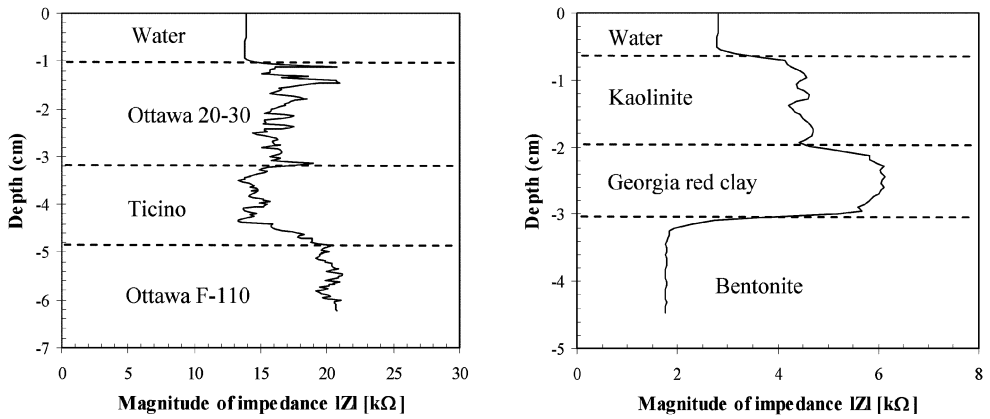

(a) Sand specimen (b) Clay specimen

Fig. 8 Stratigraphy detection with the electrical probe at f_r = 1 MHz

specimens. Two tests were performed. The first test involves a three-layer sand specimen made of Ottawa 20-30 sand (D_{50} = 0.72 mm; round), Ticino sand (D_{50} = 0.58 mm; angular), and Ottawa F-110 sand (D_{50} = 0.12 mm; round) prepared by water pluviation. The needle probe was gradually pushed into the specimen. The variation in the corrected impedance with depth is shown in Fig. 8(a). The three sand layers are distinguished. The layers with larger particles (i.e. Ottawa 20-30 and Ticino sands) exhibit higher variance than the layer composed of smaller particles (i.e. Ottawa F-110).

The second test involved kaolinite (D_{50} = 5 μm; LL = 50), Georgia red clay (D_{50} = 7 μm; LL = 40), and bentonite (D_{50} = 0.6 μm; LL = 250), each individually mixed with water at the liquid limit. Then, the water-clay mixtures were stacked in a glass container and stored for a month to reduce the possible contrast in electro chemical potential between the layers. The variation in impedance with depth was determined with the needle probe (Fig. 8b). The three clay layers are clearly distinguished. Bentonite shows the lowest variability in the impedance. The characteristic internal length scale of soils can be determined by the needle probe, for example, the distance between the thin layers in varved clays.

4.2. Void ratio and its spatial distribution

Void ratio (i.e. porosity) is an important soil property within relation to strength, conduction, and diffusion processes. Numerous attempts have been made to evaluate pore size distribution and its spatial variability, using techniques such as mercury porosimetry, gas adsorption, X-ray scattering (Mitchell, *et al*. 1976, Mulilis, *et al*. 1977), small-angle neutron scattering, computed tomography based on X-ray absorption (Desrues, *et al*. 1996), and imaging techniques using cross-sections of impregnated soils (Jang, *et al*. 1999). The mercury porosimetry and gas adsorption techniques are limited to small-size specimens. The X-ray scattering technique, which is an indirect method, requires careful calibration and usually gives qualitative information rather than quantitative information. The computed tomography method requires careful calibration and inversion techniques to smooth the contrast in mass density. Imaging techniques using cross-sections of impregnated soils are practical in sandy soils, however, its implementation is destructive and the same specimen cannot be measured both before and after testing.

A simple and effective technique is proposed herein to assess the spatial variability of sand specimens

with sub-millimetric resolution. The technique involves the needle-size probe described in the previous section. The computation of the real relative dielectric permittivity κ' (for simplicity, the term permittivity is used hereafter) from the measured impedance values $|Z^*_{meas}|$ is based on equivalent circuit elements (this approach is valid in the low frequency range, i.e. below 10 MHz). The electrical response of a soil is modeled as a 'lossy dielectric', which involves a resistor and a capacitor in parallel. Therefore, the impedance corresponding to the soil Z^*_{soil} is:

$$Z^*_{soil} = \left[\frac{1}{R_{soil}} + j\omega C_{soil}\right]^{-1} \tag{2}$$

where R_{soil} and C_{soil} are the resistance and the capacitance of the soil respectively, j is the imaginary unit, and ω is the angular frequency.

The void ratio can be estimated from the electromagnetic measurements. In its simplest form, the permittivity κ'_{mea} of saturated soils can be expressed in terms of a volumetric average. Thus, the void ratio e in saturated soils is:

$$e = \frac{\kappa'_{mea} - \kappa'_s}{\kappa'_w - \kappa'_{mea}} \tag{3}$$

where κ'_w is the permittivity of water and κ'_s is the permittivity of soil particles. The value of $\kappa'_w = 78.5$ is used for water and $\kappa'_s = 6$ for the mineral that makes the particles. Permittivity increases with void ratio in saturated soils.

Ottawa F-110 sand ($D_{50} = 0.12$ mm, $e_{max} = 0.848$, $e_{min} = 0.535$) was used to explore specimen preparation effects. Six triaxial specimens with a nominal diameter of 75 mm and height of 150 mm were prepared. A circular aluminum split mold and a 0.033 cm thick latex membrane are used to form and hold the specimen. The specimens were prepared by air pluviation, moist tamping, and water pluviation procedures.

Before triaixial testing, the electric needle probe was gradually inserted into the specimens to estimate spatial variability. The complex impedance Z^* was measured every 0.5 mm, corrected for stray parameters, and permittivity was calculated. Finally, the local void ratios were estimated from the permittivity. The results are summarized in Table 1, and some data are shown in Fig. 9 (other data can be found in Cho, *et al*. 2004). It is observed that the specimen prepared by the moist tamping method has the highest variation in void ratio, while the specimen prepared by water pluviation shows the lowest variation.

Table 1 Summary of the average void ratio and variance estimated for each specimen

Test number	Specimen preparation procedure	Average void ratio, e_{ave}	COV(%)
Test A	Air pluviation method	0.801	2.79
Test B	Moist tamping method	0.826	4.67
Test C	Water pluviation method	0.694	2.25
Test D	Air pluviation method	0.698	2.40
Test E	Moist tamping method	0.732	5.36
Test F	Water pluviation method	0.672	1.67

COV is the coefficient of variation of the estimated void ratio. The results of tests A, B and C are presented in Fig. 9 while the results of tests D, E and F can be found in Cho, *et al*. (2004).

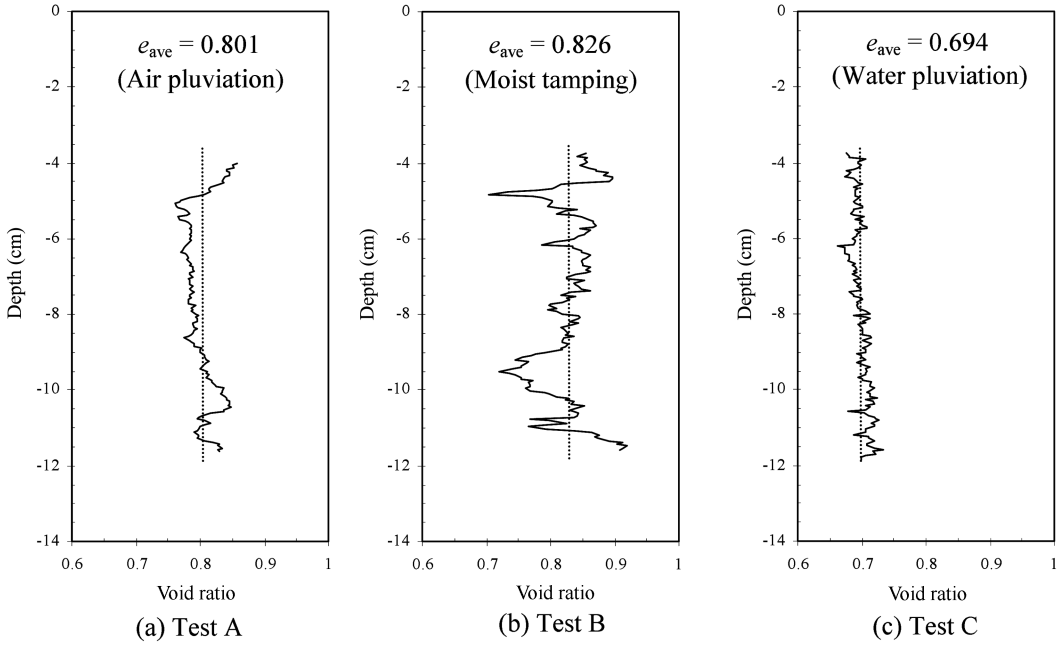

Fig. 9 Void ratio variability for different specimens (f_r = 1 MHz, voltage = 1 V). The value e_{ave} is the global void ratio of the specimen and the parenthesis represents the specimen preparation procedure

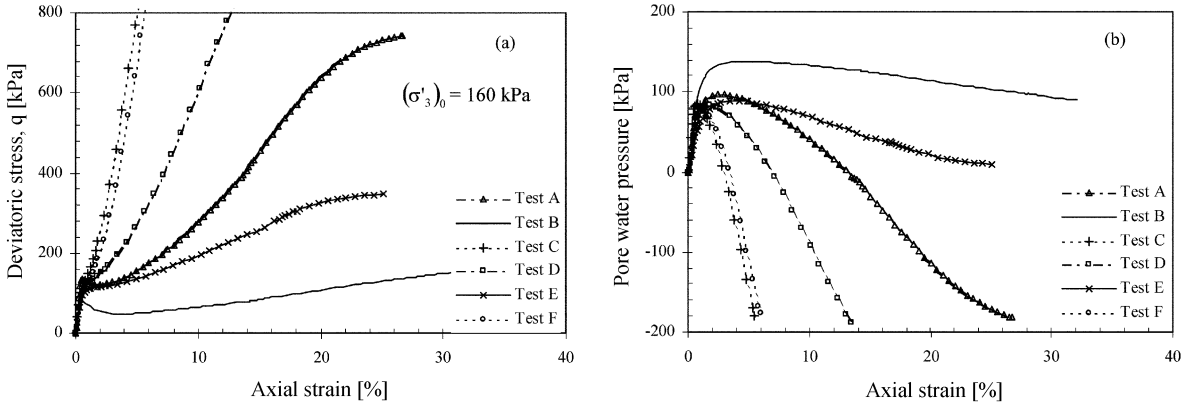

Fig. 10 Undrained triaxial test results for six specimens. Note: Initial effective confining stress is 160 kPa. Test A – Air pluviation (e = 0.780). Test B – Moist tamping (e = 0.793). Test C – Water pluviation (e = 0.656). Test D – Air pluviation (e = 0.689). Test E – Moist tamping (e = 0.722). Test F – Water pluviation (e = 0.660). The void ratios in parenthesis were the final void ratios when the specimens were subjected to the initial effective confining stress

Standard undrained triaxial tests were also performed on the specimens after electromagnetic measurements. The results are shown in Fig. 10. Comparing the result from test A to the result from test E, it is noticeable that the spatial distribution of void ratio affects the undrained strength, that is, the higher the variation in local void ratio, the lower strength.

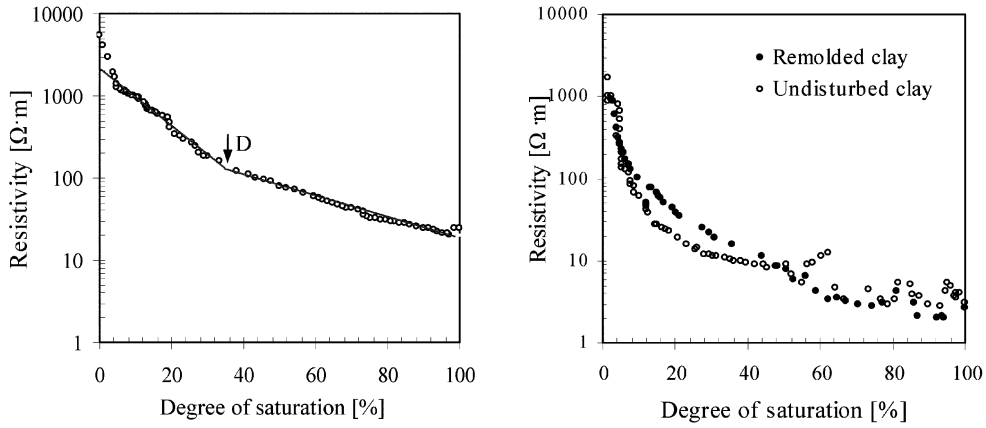

Fig. 11 The variation of resistivity with the degree of saturation

4.3. Multi-phase – unsaturated soil

The drying cell described in the previous section was used to assess the characteristics of unsaturated particulate materials with the aid of electromagnetic waves. The cell consists of an acrylic glass shell, an aluminum top platen, and an aluminum bottom platen. The metal platens, which were connected to a LCR meter with wires, acted as electrodes. This configuration allowed continuous monitoring of the electromagnetic properties of specimens made of two soils. The LCR meter was used to gain low frequency electromagnetic properties (e.g. resistance and reactance; the resistivity ρ can be calculated from the relation of $\rho = R \cdot L/A$ where R is the resistance, L is the specimen length, and A is the specimen area). The tested soils were Pusan clay and Keum River sand. The void ratio of the natural sand specimen was $e = 0.76$, and the void ratio of the undisturbed clay specimen was the same as that of the reconstituted specimen with $e = 1.76$.

The resistivity (ρ) of each specimen is plotted versus the corresponding the degree of saturation. When the degree of saturation decreases, the resistivity increases in both specimens. The resistivity in the sand specimen increases continuously with the decrease of water content (Fig. 11a). The air-entry value in the water-retention curve cannot be detected from resistivity measurements, suggesting that the percolation of the air phase minimally affects the variation in resistivity. The resistivity-degree of saturation trend is represented by a bi-linear line. The transition point D, at the intersection of these two lines, is related to the percolation threshold, which is the critical water fraction when the continuous phase becomes disconnected (i.e. completion of pendular stage).

The resistivity in the clay specimens increases continuously with the decrease in saturation (Fig. 11b). Contrary to the sand specimen, the resistivity of the clay specimens fluctuates significantly at high degrees of saturation. This abnormal result may be related to water flux and unbalanced pressure homogenization during drying or shrinkage of the specimen, but further study is required. It is observed that at low degrees of saturation, the fluctuation of resistivity disappears and the connectivity of the water in the undisturbed specimen is more pronounced than that of the remolded specimen. The resistivity of soil-water mixtures is dependent on the degree of saturation, thus, the presence of water and the interaction between the water and soil particles in unsaturated media can be assessed using electromagnetic measurements.

5. Summary and conclusions

Soils are particulate and multi-phase materials, thus, their behavior is governed by microscale characteristics, effective stress, the presence of water, global void ratio, and temporal and spatial scales. These properties can be effectively characterized using wave-based techniques. Experiments were performed using both elastic and electromagnetic waves to facilitate the application of wave-based techniques to characterize particulate materials. The first application involved shear waves and centered on monitoring changes in effective stress during consolidation, multi-phase phenomena related to capillarity, and microscale characteristics of particles. The second application involved electromagnetic waves focusing on stratigraphy detection in layered soils, the estimation of the void ratio and its spatial distribution, and conduction in unsaturated soils. The main conclusions from this study are as follows:

- When a clay is subjected to a K_o-loading, the shear wave velocity is uniquely related to the state of stress, so that it can be used to assess the state of stress and its changes during the consolidation.
- In unsaturated soils, changes in stiffness are related to changes in interparticle forces such as capillarity, bonding due to ion sharing, buttress effects due to fines migration and cementation due to salt precipitation. Shear waves permit studying the evolution of effective interparticle forces in unsaturated soils. This is particularly valuable in the pendular regime where direct measurements of the negative pore-water pressure are not feasible.
- Angular and non-spherical particles increase the sensitivity of stiffness to the state of stress, rendering high β-exponents.
- As the degree of saturation decreases, the shear wave velocity and resistivity in unsaturated soils increase continuously and show no drop at the perfectly dry condition. The relation of shear wave velocity and resistivity to the degree of saturation is unique for each soil, underlining the importance of water content on soil characterization.
- The pore fluid and the mineralogy of grains govern the resistivity of saturated soils, and the amount of water in the soil mass and its connectivity controls resistivity changes in unsaturated soils.
- The electrical needle-size probe can be used to detect interfaces in layered soils and to effectively assess the spatial distribution of void ratio in saturated soils and other properties in laboratory specimens, with sub-millimetric resolution. The local measurements of complex impedance permit assessing the spatial variability of either porosity, fluid resistivity (i.e. water content), or both.
- Overall, the shear wave measurements allow studying the evolution of effective stress in unsaturated soils as well as in saturated soils while the electromagnetic wave measurements give insight into conduction processes and allow estimating void ratio and its spatial distribution in saturated soils.

Acknowledgements

This research was supported by the Young Scientist Research Program (Grant No. R08-2003-000-10452-0) under the KOSEF. Prof. Carlos Santamarina in Georgia Tech provided valuable information and comments. The authors are very thankful to reviewers for their detailed reviews.

References

Barrett, P. J. (1980), "The shape of rock particles, a critical review", *Sedimentology*, **27**, 291-303.
Cho, G. C. (2001), *Unsaturated soil stiffness and post-liquefaction shear strength*, Ph.D. Thesis, Georgia Institute of

Technology, 288.
Cho, G. C. and Santamarina, J. C. (2001), "Unsaturated particulate materials - Particle-level study", *J. Geotech. Geoenviron. Eng.*, ASCE, **127**(1), 84-96.
Cho, G. C., Lee, J. S., and Santamarina, J. C. (2004), "Spatial variability in soils: high resolution assessment with electrical needle probe", *J. Geotech. Geoenviron. Eng.*, ASCE, **130**(8), August, 843-850.
Desrues, J., Chambon, R., Mokni, M., and Mazerolle, F. (1996), "Void ratio evolution inside shear bands in triaxial sand specimens studied by computed tomography", *Géotechnique*, **46**(3), 529-546.
Dobry, R. and Petrakis, E. (1990), "Micromechanical modeling to predict sand densification by cyclic straining", *J. Eng. Mech.*, ASCE, **116**(2), 288-308.
Fenton, G. A. and Griffiths, D. V. (1996), "Stochastics of free surface flow through stochastic earth dam", *J. Geotech. Eng.*, **122**(6), 427-436.
Fredlund, D. G. and Rahardjo, H. (1993), *Soil Mechanics for Unsaturated Soils*. Wiley Inter-Science, New York, 517.
Frossard, E. (1979), "Effect of sand grain shape on interparticle friction: indirect measurements by Rowe's stress dilatancy theory", *Géotechnique*, **29**(3), 341-350.
Griffiths, D. V. and Fenton, G. A. (1993), "Seepage beneath water retaining structures founded on spatially random soil", *Géotechnique*, **43**(4), 577-587.
Heyman, J. (1997), *Coulomb's Memoir on Statics*, An Essay in the History of Civil Engineering, Imperial College Press, p. 212.
Jang, D.-J., Frost, J. D., and Park, J. Y. (1999), "Preparation of epoxy impregnated sand coupons for image analysis", *Geotech. Testing J.*, GTJODJ, **22**(2), 147-158.
Krumbein, W. C. and Sloss, L. L. (1963), *Stratigraphy and Sedimentation*, Second Edition, W. H. Freeman and Company, San Francisco, 660.
Kuo, C.-Y., Frost, J. D., Lai, J. S., and Wang, L. B. (1996), "Three-dimensional image analysis of aggregate particle from orthogonal projections", *Transportation Research Record*, **1526**, 98-103.
Mitchell, J. K., Chatoian, J. M., and Carpenter, G. C. (1976), *The influences of sand fabric on liquefaction behavior*, Report No. TE 76-1, U.S. Army Engineer Waterways Experiment Station, University of California, Berkeley.
Mulilis, J. P., Seed, H. B., Chan, C. K., Mitchell, J. K., and Arulanandan, K. (1977), "Effects of sample preparation on sand liquefaction", *J. Geotech. Eng.*, **103**(GT2), 91-108.
Paice, G. M., Griffiths, D. V., and Fenton, G. A. (1996), "Finite element modeling of settlements on spatially random soil", *J. Geotech. Eng.*, ASCE, **122**(9), 777-779.
Pennington, D. S., Nash, D. F. T., and Lings, M. L. (1997), "Anisotropy of shear stiffness in Gault clay", *Géotechnique*, **47**(3), 391-398.
Popescu, R. and Prevost, J. H. (1996), "Influence of spatial variability of soil properties on seismically induced soil liquefaction", *Uncertainty in the Geological Environment: from theory to practice, Proceedings of Uncertainty '96*, edited by Schackelford et al., Geotechnical Special Publication **58**(2), 1098-1112.
Popescu, R., Prevost, J. H., and Deodatis, G. (1997), "Effects of spatial variability on soil liquefaction: some design recommendations", *Géotechnique*, **47**(5), 1019-1036.
Powers, M. C. (1953), "A new roundness scale for sedimentary particles, *J. Sedimentary Petrology*, **23**(2), 117-119.
Roscoe, K. H., Schofield, A. N., and Wroth, C. P. (1958), "On the yielding of soils", *Géotechnique*, **8**, 22-53.
Santamarina, J. C. and Cho, G. C. (2004), "Soil behaviour: the role of particle shape", *The Skempton Memorial Conference*, Thomas Telford, **1**, 604-617.
Santamarina, J. C. and Cascante, G. (1998), "Effect of surface roughness on wave propagation parameters", *Géotechnique*, **48**(1), 129-136.
Santamarina, J. C., Klein, K. A., and Fam, M. A. (2001), *Soils and Waves – Particulate Materials Behavior, Characterization and Process Monitoring*, John Wiley and Sons, LTD, 488.
Santamarina, J. C., Rinaldi, V. A., Fratta, D., Klein, K., Wang, Y. H., Cho, G. C., and Cascante, G. (2004), The properties of near-surface soils in relation to elastic and electromagnetic wave parameters, Chapter in *Physical properties of near-surface materials*, in print.
Schofield, A. N. (1998), "Don't use the C word," *Ground Engineering*, August, 30-32.
Schofield, A. N. and Wroth, P. (1968), *Critical State Soil Mechanics*, McGraw-Hill Book Company, 310.
Stokoe, K. H., II, Lee, J. N.-K. and Lee, S. H.-H. (1991), "Characterization of soil in calibration chambers with

seismic waves", *Proceedings of 1st International Symposium on Calibration Chamber Testing*, Elsevier, Potsdam, New York, 363-376.
Tonon, F., Bernardini, A., and Mammino, A. (2000), "Reliability analysis of rock mass response by means of random set theory", *Reliability Engineering and System Safety*, **70**(3).
Wadel, H. (1932), "Volume, shape, and roundness of rock particles", *J. Geology*, **40**, 443-451.
Yimsiri, S. and Soga, K. (1999), "Effect of surface roughness on small-strain modulus: micromechanics view", *Pre-failure Deformation Characteristics of Geomaterials: Proceedings, 2nd International Symposium*, Torino, Italy; edited by M. Jamiolkowski, R. Lancellotta, and D. Lo Presti, 597-602.
Yong, R. N., Alonso, E., and Tabba, M. M. (1977), "Application of risk analysis to the prediction of slope stability", *Canadian Geotech. J.*, **14**, 540-553.
Yudhbir, and Abedinzadeh, R. (1991), "Quantification of particle shape and angularity using the image analyzer", *Geotechnical Testing J.*, GTJODJ, **14**(3), 296-308.

CC